

Three-Dimensional Simulations of Richtmyer-Meshkov Experiments

R.M. Hueckstaedt¹, S.H. Batha, M.M. Balkey, N.D. Delamater, J.R. Fincke, R.L. Holmes, N.E. Lanier, G.R. Magelssen, J.M. Scott, and J.M. Taccetti

Los Alamos National Laboratory, Los Alamos, NM, USA

C.J. Horsfield, K.W. Parker, and S.D. Rothman

Atomic Weapons Establishment, Aldermaston, Berkshire, UK

ABSTRACT

Instabilities play an important role in driving the evolution of hydrodynamic systems on scales ranging from those of inertial confinement fusion capsules to interstellar turbulence. We have conducted experiments at the Omega laser facility to examine Richtmyer-Meshkov instabilities in a convergent plasma. Cylindrical targets consisting of a low-density foam core and an aluminum marker layer within an epoxy ablator are directly driven by fifty laser beams and radiographed along the axis. The outer surface of the aluminum layer is machined in order to examine the evolution of different perturbation spectra. Experiments and simulations study unperturbed (smooth), single-mode, multi-mode (rough), and multi-mode with particular modes accentuated (specified-rough) surfaces. The experimental results differ for rough and specified-rough targets. The rough targets show no marker layer growth beyond that of the smooth targets; whereas, the specified-rough targets (and the single-mode targets) show additional marker growth. Two-dimensional simulations using the RAGE code predict additional marker growth for all perturbed targets and do not explain the lack of observed growth for rough surfaces. We have expanded our simulation efforts to include three-dimensional simulations. At issue is whether the two-dimensional contributions to the specified-rough spectra lead to an enhanced growth of large-scale features not generated by the rough spectra. In this paper we present our latest results contrasting the two-dimensional and three-dimensional simulations. We find that a transition from 2-d to 3-d does not bring numerical results into agreement with the experimental results.

¹rmhx@lanl.gov

1. Introduction

Hydrodynamic instabilities play a key role in processes ranging from the small (μm) scales of ICF experiments to the large (*parsec*) scales of supernova explosions and galactic dynamics. Two prominent types are the Rayleigh-Taylor (RT) and Richtmyer-Meshkov (RM) instabilities across a density interface. The Rayleigh-Taylor instability occurs when pressure and density gradients across an interface act in opposite directions (Rayleigh 1883; Taylor 1950). The RM is an impulsively driven instability which occurs when perturbations are amplified as a shock refracts through an interface (Richtmyer 1960; Meshkov 1969). Both experience a period of linear growth before secondary Kelvin-Helmholtz instabilities give rise to a nonlinear phase and the familiar “mushroom cap” morphology. Despite the similarities in structure, the RT and RM instabilities have distinct growth rates and driving mechanisms. We seek to study RM instabilities in a convergent geometry through a series of Omega laser experiments and hydrodynamic simulations.

2. Experiment

Experiments were conducted to study RM mixing in convergent geometry using cylindrical targets at the OMEGA laser facility at the Laboratory for Laser Energetics of the University of Rochester (Lanier et al. 2003; Fincke et al. 2004a). The targets were composed of a foam inner core and an outer layer of epoxy, with a thin (nominally $8\mu\text{m}$) aluminum marker layer in between (Figure 1). They measured about 2mm in length and 1mm in diameter. Fifty laser beams were used to directly ablate the outer layer of epoxy and drive an approximately Mach 10 shock through the aluminum marker layer. The drive was configured such that the marker acceleration after shock passage was minimal, allowing us to eliminate the RT instability and concentrate on the RM instability. We used an iron backlighter to generate radiographs along the cylindrical axis. We measure the width of the aluminum marker layer (which appears as a minimum transmission region) as a function of time for our primary diagnostic. It is important to note that the interpretation of the experimental radiographs has evolved. In this communication, we refer to the original results reported by Lanier et al. (2003). They used the 50% transmission points as their criterion for determining marker widths. Fincke et al. (2004b) have utilized a different analysis which measures the inner and outer widths separately through upper and lower line-averaged density thresholds. Further information about the experimental diagnostics and the new analysis techniques is given by Fincke et al. (2004b). A description of similar experiments using double cylinders is given by Parker et al. (2004).

We examined different types of perturbation spectra by machining perturbations onto the outer surface of the aluminum markers. Spectral types included smooth (unperturbed), single mode,

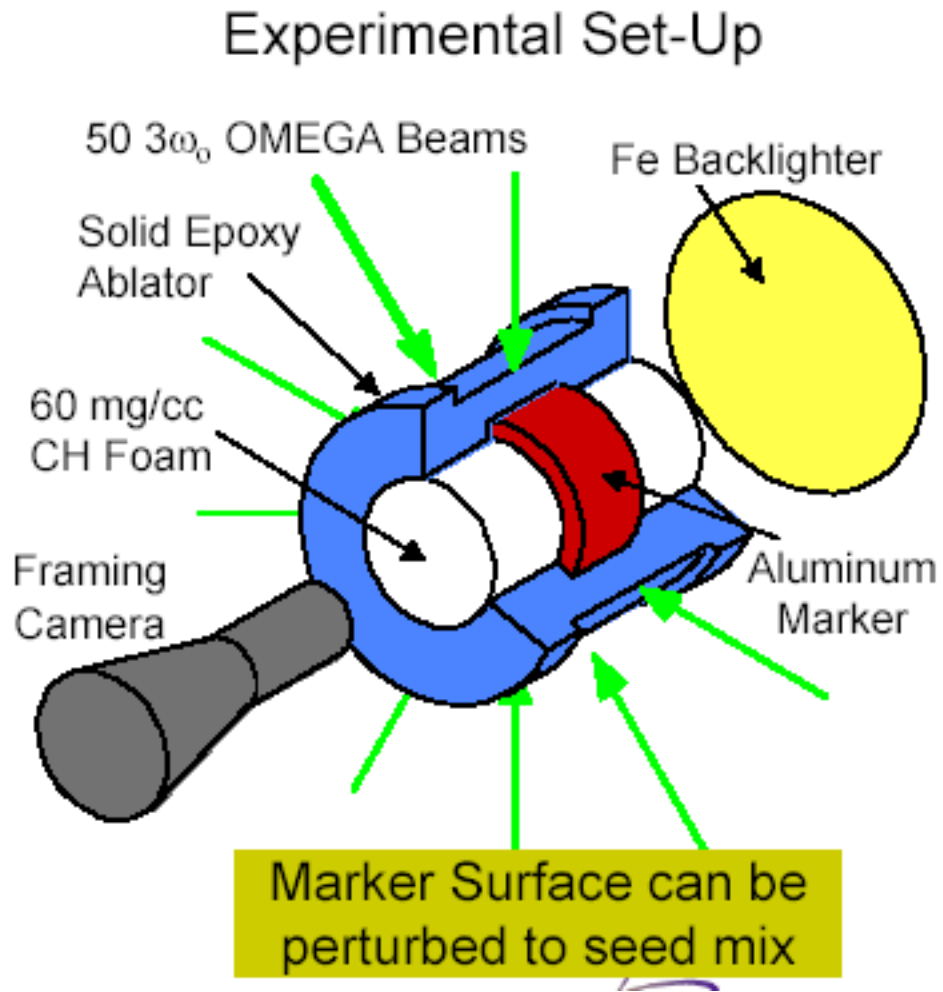


Fig. 1.— Cartoon of cylindrical target and diagnostic orientation.

rough (multi-mode), and specified-rough (multi-mode with a high power single-mode component). We term large amplitude rough markers “super-rough”. In this study, we emphasize a super-rough and a specified-rough case. The specified-rough has a strong peak in its power spectrum at $\lambda = 9.38\mu\text{m}$ (Figure 2), but the super-rough contains more overall power.

Expectations prior to the experiment were that all perturbed markers would show marker growth larger than that of the smooth markers. However, according to the results of Lanier et al. (2003), additional growth is observed for the single-mode and specified-rough targets but not for the rough targets. We use numerical simulations to explore the apparent lack of growth for the rough markers.

3. Simulations

We use the RAGE (Radiation Adaptive Grid Eulerian) code to investigate different perturbation spectral types. RAGE is an Eulerian hydrocode which uses a second order Godunov scheme. Continuous adaptive mesh refinement is performed on a cell by cell basis to allow increased resolution in areas of interest. Laser ray trace and post processing capabilities are still under development, so we use time dependent internal energy sources to approximate laser energy deposition and material preheats. We determine the values for the energy sources by simulating a smooth marker layer target with the LASNEX code and calibrating RAGE to match. We impose perturbations to the marker layer either through a combination of cosines (for 2-d simulations) or by mapping target surface measurements directly onto the computational grid (for 3-d). Since simulated output does not include the effects of imaging and motion blur, we do not attempt to make direct comparisons between experimental and numerical results at this time. Rather, we seek to explain the qualitative experimental result that single-mode and specified-rough markers grow more than smooth markers while super-rough markers do not.

We perform 2-d simulations in cylindrical geometry and observe marker growth beyond that of the smooth marker case for all perturbed models. Marker widths are measured in the simulations by forming line averages of aluminum volume fraction and measuring the distance between the 5% contours. A possible reason for discrepancies between experiments and simulations is the simulations’ lack of heating to the Al layer prior to shock arrival. We add preheat to the RAGE simulations by first determining the energy profile as a function of time in the aluminum in a LASNEX calculation. We then translate this information into an additional set of internal energy sources within the aluminum layer. When added to a smooth marker simulation, preheat causes an expansion to the Al which persists after shock arrival as a slightly thicker marker. This same expansion causes perturbed markers to lose definition and flatten out before shock arrival, resulting in a smaller amplitude and slower RM growth. The decrease in marker growth can be significant

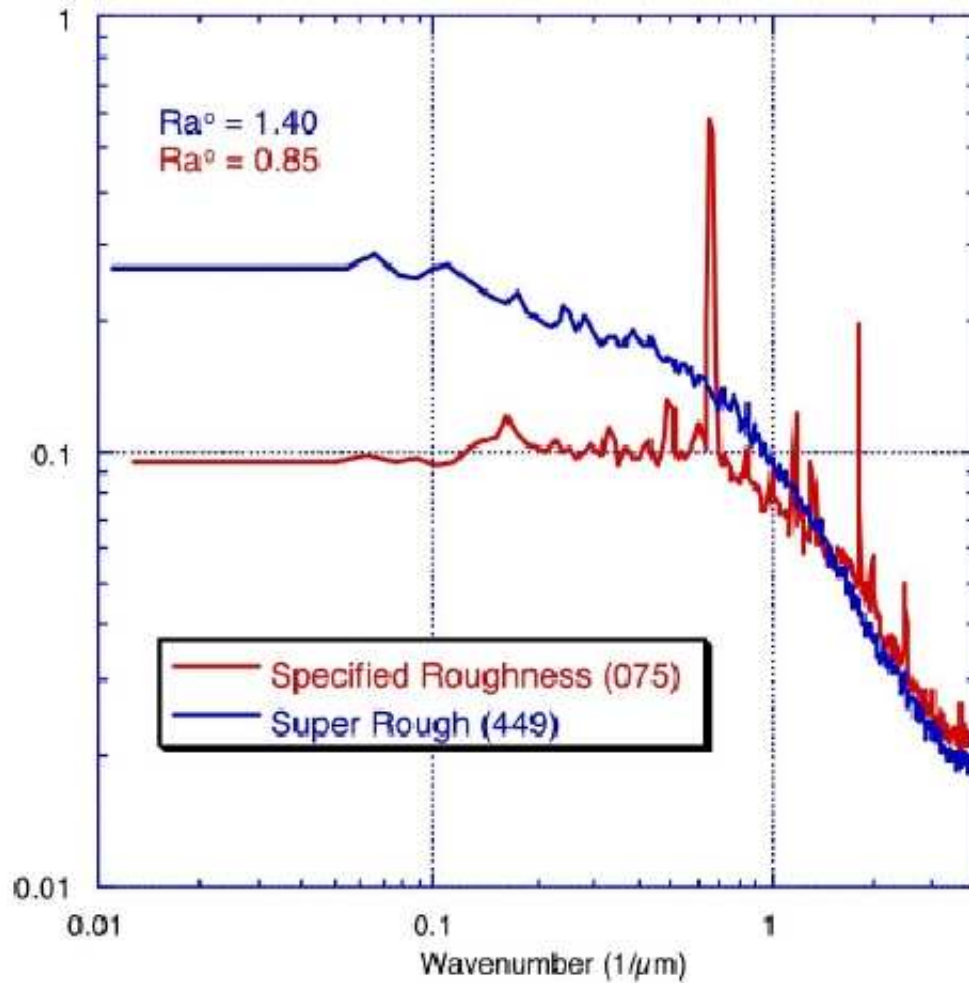


Fig. 2.— Specified-rough (red) and super-rough (blue) perturbation spectra on the outer aluminum surface. Amplitude is plotted as a function of wavenumber.

(a typical value is 20%), but it is not enough to bring the 2-d simulations into agreement with the experiments. Furthermore, the addition of Al preheat decreases growth in both rough and specified-rough markers (Figure 3), so preheat alone cannot account for the differences between these types of markers observed experimentally.

Another possible reason for differing experimental and numerical results is that 2-d simulations do not adequately model the 3-d physical behavior of the experiments. In 2-d calculations, all perturbations are approximated as 2-d surfaces. This is sufficient for single-mode calculations but fails to realistically model 3-d rough perturbations. The specified-rough spectrum has a strong 2-d component superimposed on a 3-d roughness. It may be that this 2-d component gives the specified-rough marker a 2-d behavior that more closely resembles the behavior of single-mode markers rather than rough markers. Theories hold that the dominant mode of energy transfer in complex flows is different in 2-d and 3-d. In 2-d, the dominant mode is from small scale to large scale; whereas, energy preferentially flows from large to small scales in 3-d (Kraichnan and Montgomery 1980). It is unclear whether the flows we consider reach a state of sufficient complexity to obey this dichotomy of behavior.

We compare 2-d and 3-d simulations in search of a difference in behavior. Since modeling the full cylindrical geometry in 3-d would require an extremely large expenditure of computing resources, we reduce the experimental geometry to a Cartesian shock tube configuration (Figure 4). The effects of convergence upon RM growth is removed from the problem, but differences due to perturbation spectra should remain. We also leave out preheats so as to concentrate solely on perturbation spectra. The representation for the laser deposition remains the same. The grid setup involves removing the curvature from target surface measurements and mapping out $96\mu\text{m} \times 96\mu\text{m}$ planar sections.

The 3-d structure of the marker layer over time for the specified-rough (Figures 5 – 10) and super-rough (Figures 11 – 16) cases are shown as altitude plots in which the color scale represents the position on the grid. The red end of the color scale (highest x value) is the side that is shocked first. Three different orientations are shown in each figure. Only those cells containing a threshold volume fraction (nominally 15%) of aluminum are shown. At time zero, the dominant $9.38\mu\text{m}$ mode in the specified-rough case is clearly evident. The super-rough marker lacks such a mode, but it does show several large peaks. By $t = 1\text{ ns}$ the shock has compressed the marker layers, which alters the perturbation amplitudes but not their shapes. Once the shock has passed and the markers are set into motion, the perturbations grow on the trailing edge. Due to the finite thickness of the marker layer, the shock also gives rise to feed-through structures which grow on the leading edge. It is with regard to the feed-through that we see the only large difference between the evolution of the specified-rough and super-rough markers. The specified-rough marker shows a stronger feed-through phenomenon. As the shock passes through the perturbed outer edge of

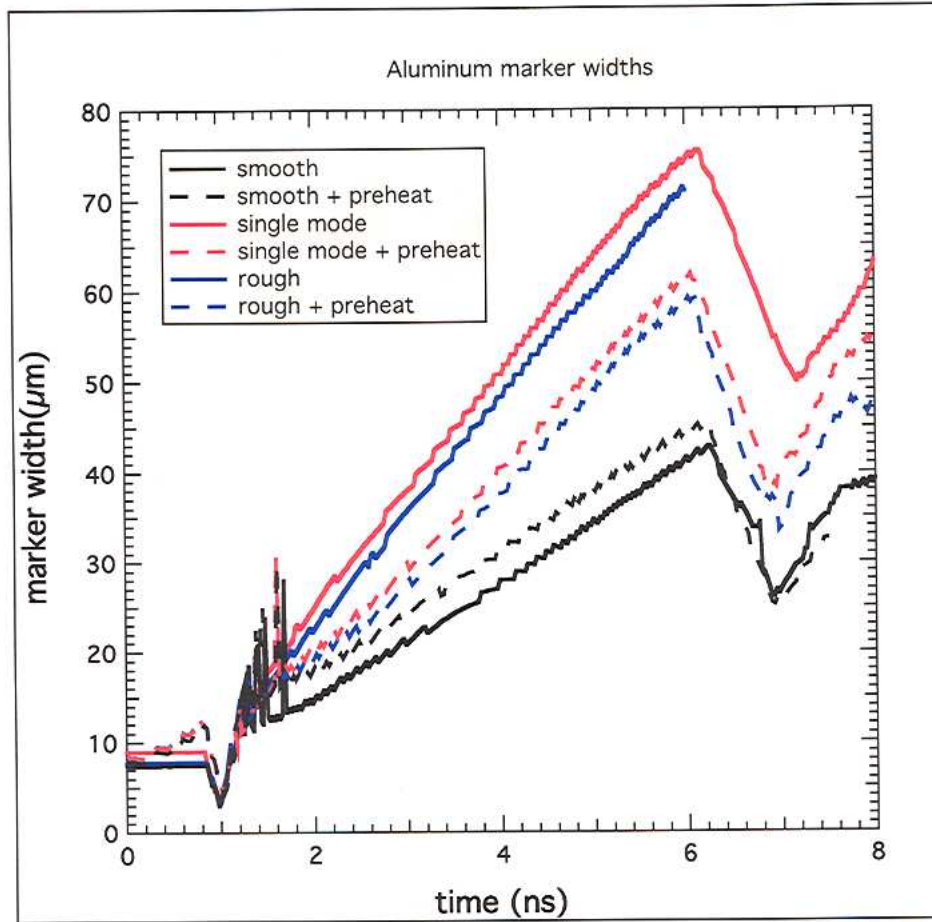


Fig. 3.— Simulated marker-width evolution for 2-d cylindrical cases. Results for single-mode simulations are shown in place of those for specified-rough simulations. The solid lines are results without preheat to the aluminum marker and the dashed lines those with preheat.

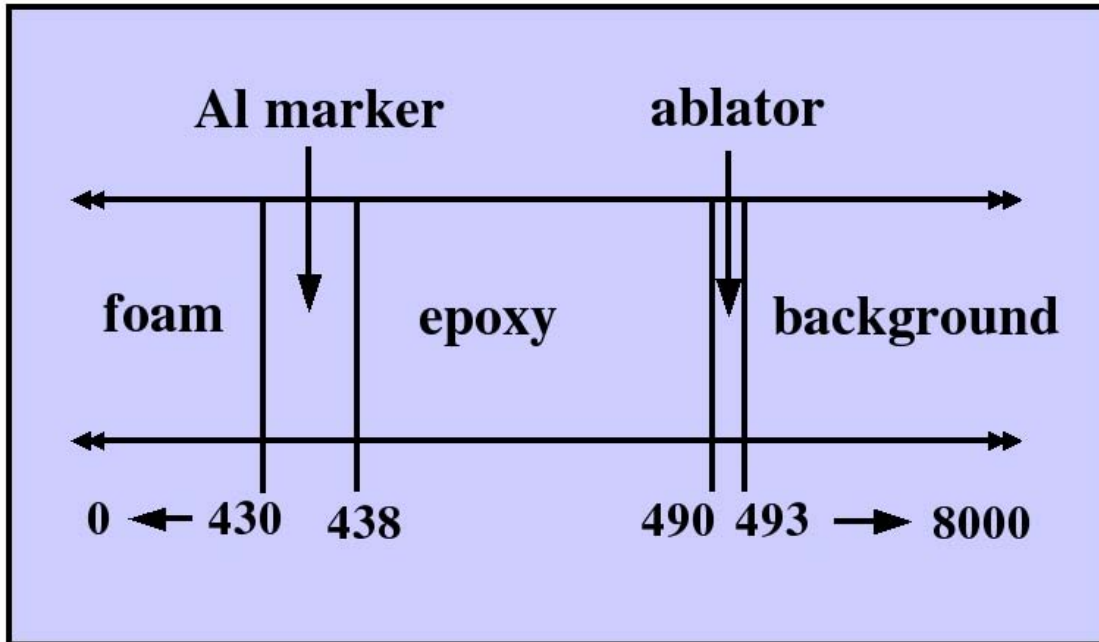


Fig. 4.— Shock tube geometry for 3-d simulations. Convergence is removed, but the radial dimensions of the experiment are preserved. The numbers give the position of each interface in microns. The grid is extended to $8000\mu m$ in order to avoid boundary effects.

the specified-rough marker, it is imparted with the 2-d component of the perturbation spectrum. Having the wavelength ($9.38\mu\text{m}$) near in value to the marker thickness ($8\mu\text{m}$) aids the shock in forming coherent structure on the leading edge. In the case of the super-rough marker, the shock is refracted into the aluminum in a less coherent manner, resulting in a less structured shock front as it exits the marker. This translates into a smaller effective amplitude and hence less leading-edge RM growth than in the specified-rough case. The main result from the 3-d simulations is one of omission; there is no evidence that the 3-d structure cascades to smaller scale structure not seen in 2-d simulations.

Overall marker widths are extracted and compared versus time in Figure 17. In addition to the 3-d specified-rough and super-rough, 2-d results for the specified-rough are shown. Even with a lesser amount of feed-through, the higher initial amplitude of the super-rough case causes it to out grow the specified-rough case. The 2-d cylindrical specified-rough case includes convergence, so it grows more than the planar cases. Interestingly, the 2-d planar specified-rough case agrees at early times with the 3-d super-rough case before falling in line with the 3-d specified-rough case. This is likely due to the different manners in which the perturbation spectra are applied in 2-d and 3-d. Instead of a direct mapping as in 3-d, the 2-d perturbations are composed of an artificial set of cosine terms (312 in this case) configured to approximate the overall power spectrum from the 3-d surface measurements. This procedure can result in a higher peak amplitude in the 2-d specified-rough case than that in the 3-d specified-rough case. Of more importance than any early-time differences due to variations in spectra is the observation that at the diagnostic time for the experiment (typically $3\text{-}7\text{ns}$), the simulated marker growth for the 2-d and 3-d specified-rough markers are indistinguishable.

4. Conclusions

Understanding how hydrodynamic instabilities evolve is crucial for understanding many physical systems. We have performed experiments on the Omega laser and are running two and three dimensional simulations with RAGE in order to help understand the growth of Richtmyer-Meshkov instabilities. We find that allowing preheat to the aluminum marker layer typically reduces marker growth by about 20% in 2-d simulations, but not enough to bring simulations in line with experimental results. Our 3-d simulations without preheats have also failed to match the originally reported experimental results. A new set of 3-d simulations including aluminum preheat is underway.

The experimental results vary depending upon the type of analysis performed. In their original analysis, Lanier et al. (2003) measured the entire marker width using the 50% transmission points. They concluded that the evolution of the rough and specified-rough markers differ. The new

analysis method of Fincke et al. (2004b) for the experimental data leads to a different conclusion. Instead of determining the total marker width, they measure just the trailing-edge growth using a density threshold value. They find no discernable difference in behavior between the specified-rough and super-rough marker targets. This brings the simulations into qualitative agreement with the experiments, since the large differences between the different simulated marker types appear as feed-through on the leading edge.

Regardless of how the simulations compare to experiments, the lack of variation between 2-d and 3-d simulations indicates that either planar RM mixing in this physical environment is not quenched by allowing an additional degree of freedom for vortex formation, or these simulations do not adequately show the differences between 2-d and 3-d behavior. Possible shortcomings (such as numerical resolution, k -space coverage, physics coverage, and lack of convergence in 3-d) are being investigated.

This work was performed under the auspices of the U.S. Department of Energy by the University of California at Los Alamos National Laboratory under contract No. W-7405-Eng-36.

REFERENCES

- Fincke, J.R., Lanier, N.E., Batha, S.H., Hueckstaedt, R.M., Magelssen, G.R., Rothman, S.D., Parker, K.W., and Horsfield, C.J.:2004, Postponement of Saturation of the Richtmyer-Meshkov Instability in a Convergent Geometry, *Physical Review Letters*, in press.
- Fincke, J.R., Lanier, N.E., Batha, S.H., Taccetti, J.M., Hueckstaedt, R.M., Magelssen, G.R., Delamater, N.D., Rothman, S.D., Parker, K.W. and Horsfield, C.J.:2004, Postponement of Saturation of the Richtmyer-Meshkov Instability by Convergence, *these proceedings*.
- Kraichnan, R.H. and Montgomery, D.:1980, Two-dimensional Turbulence, *Reports on Progress in Physics*, **43**, 547–619.
- Lanier, N.E., Barnes, C.W., Batha, S.H., Day, R.D., Magelssen, G.R., Scott, J.M., Dunne, A.M., Parker, K.W. and Rothman, S.D.:2003, Multi-Mode Seeded Richtmyer-Meshkov Mixing in a Convergent, Compressible, Miscible Plasma System, *Physics of Plasmas*, **10**, 1816–1821.
- Lord Rayleigh: 1883, Investigation of the Character of the Equilibrium of an Incompressible Heavy Fluid of Variable Density, *Proc.Roy.Math.Soc.*, **14**, 170.
- Meshkov, E.E.:1969, Instability of the Interface of Two Gases Accelerated by a Shock Wave, *Fluid Dynamics*, **43**, 101-104.

Parker, Kenneth, Horsfield, C.J., Rothman, S.D., Balkey, M.M., Batha, S.H., Delamater, N.D, Fincke, J.R., Hueckstaedt, R.M., Lanier, N.E., Magelssen, G.R. and Taccetti, J.M. :2004, Investigation of Mix after Reshock in a Cylindrical Geometry, *these proceedings*.

Richtmyer, R.D.:1960, Taylor Instability in Shock Acceleration of Compressible Fluids, *Comm. Pure and Applied Math.*, **13**, 297–319.

Taylor, G.I.:1950, The Instability of Liquid Surfaces when Accelerated in a Direction Perpendicular to their Planes, *Proc.Roy.Soc.London A*, **201**, 192.

This report was prepared with the AAS L^AT_EX macros v5.2.

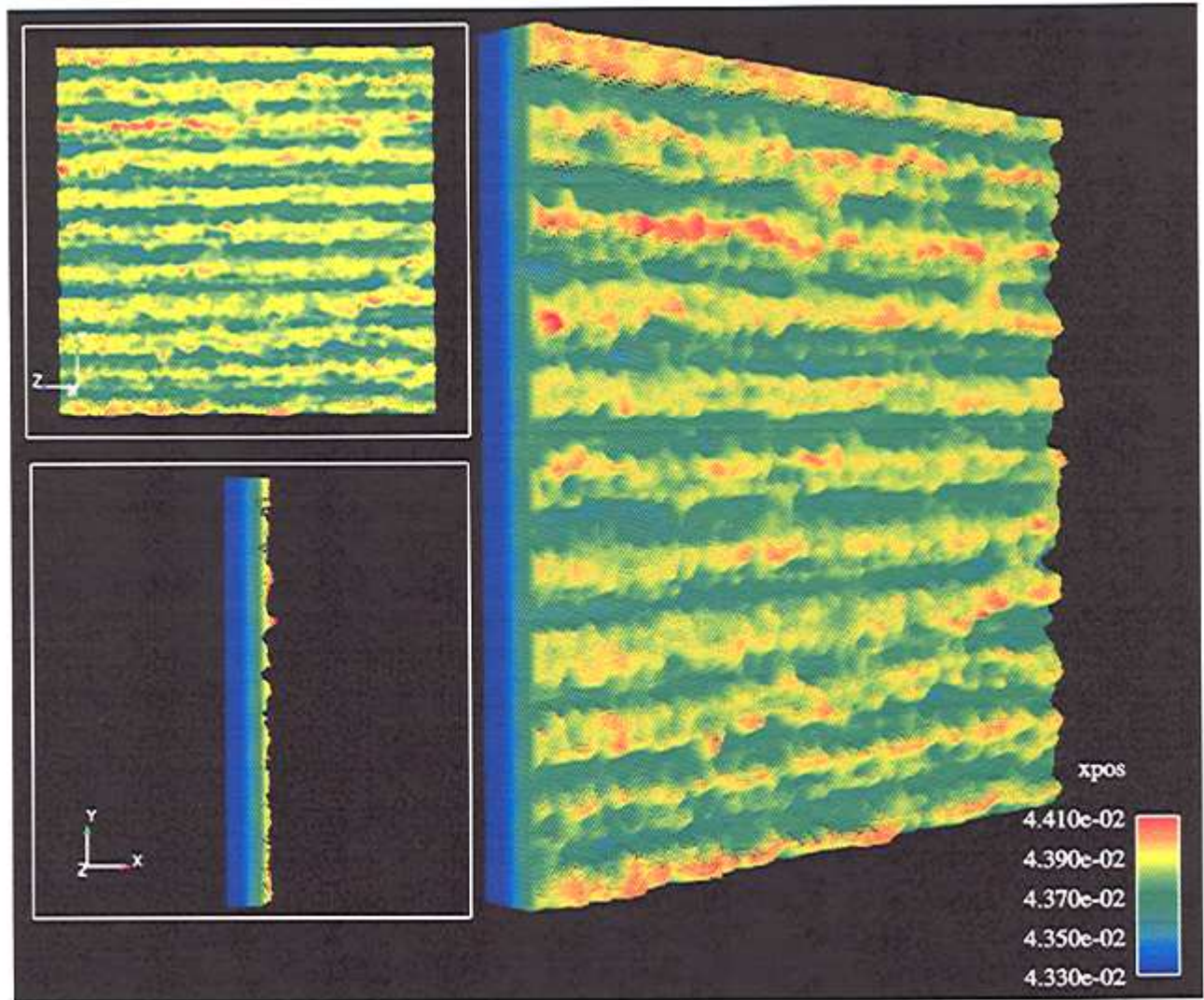


Fig. 5.— Altitude plot showing the specified-rough marker at $t = 0$ ns. The color scale shows the x position along the shock tube. The shock passes through the marker in the $-x$ direction.

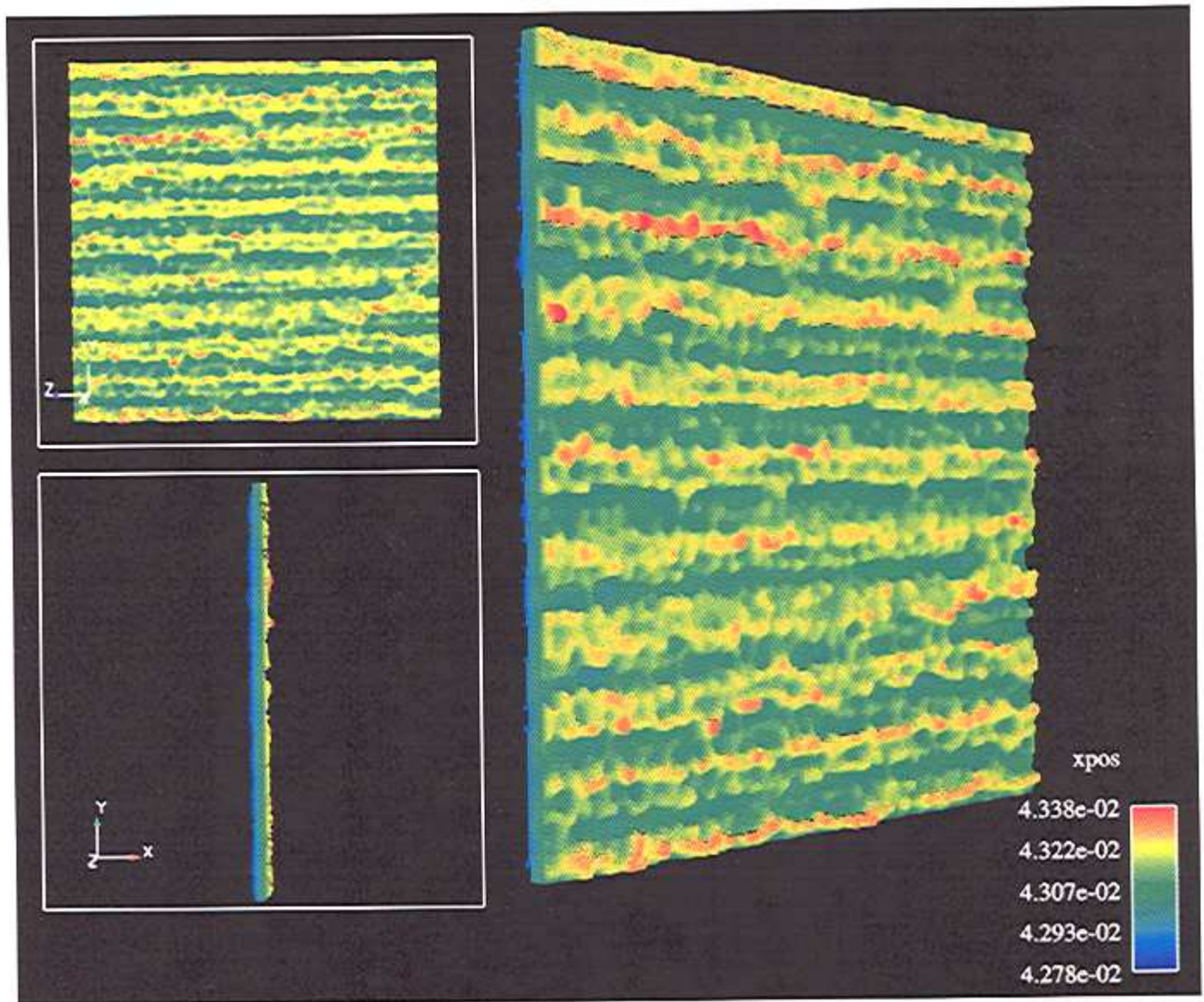


Fig. 6.— Altitude plot showing the specified-rough marker at $t = 1 \text{ ns}$.

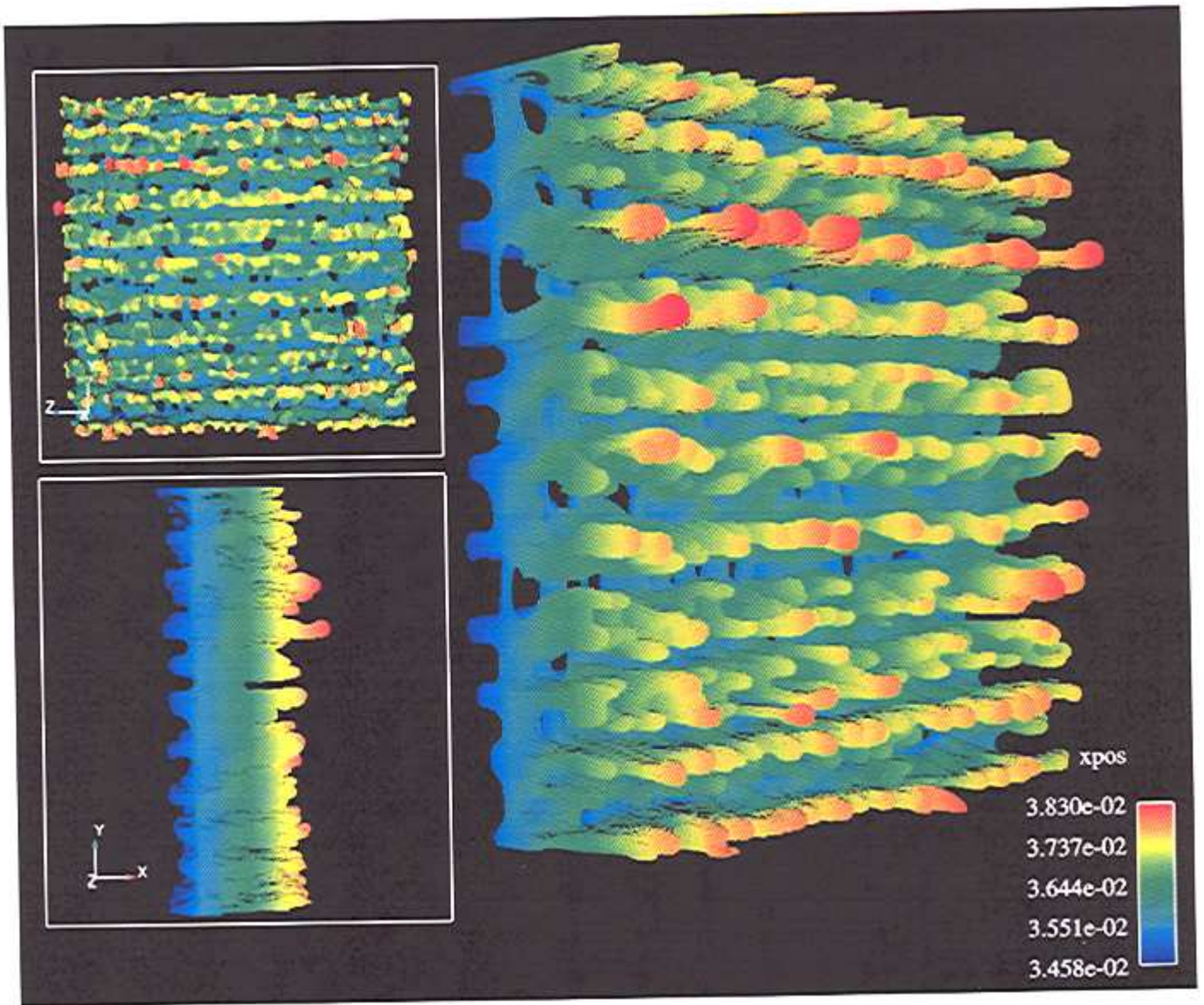


Fig. 7.— Altitude plot showing the specified-rough marker at $t = 2 \text{ ns}$.

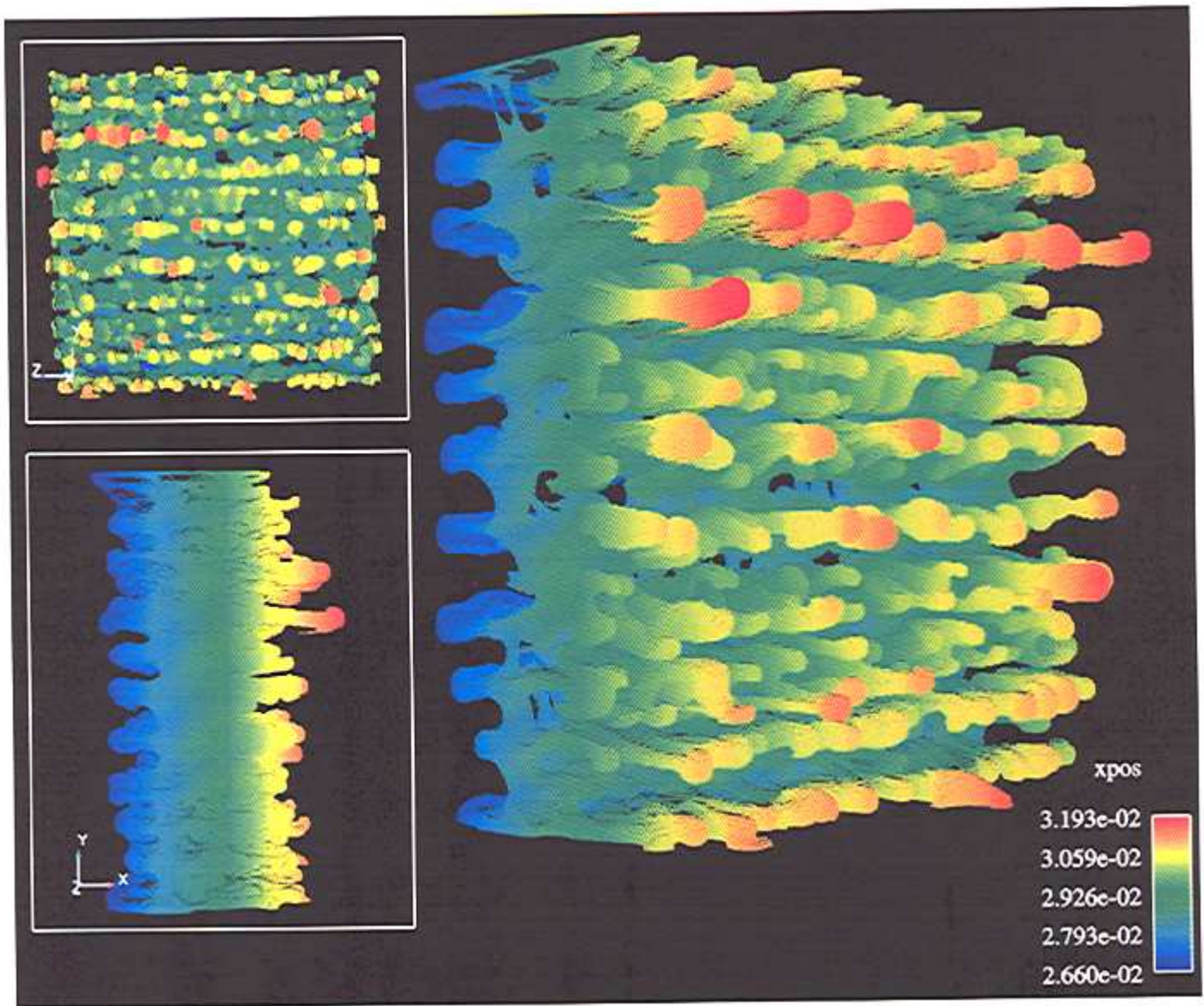


Fig. 8.— Altitude plot showing the specified-rough marker at $t = 3 \text{ ns}$.

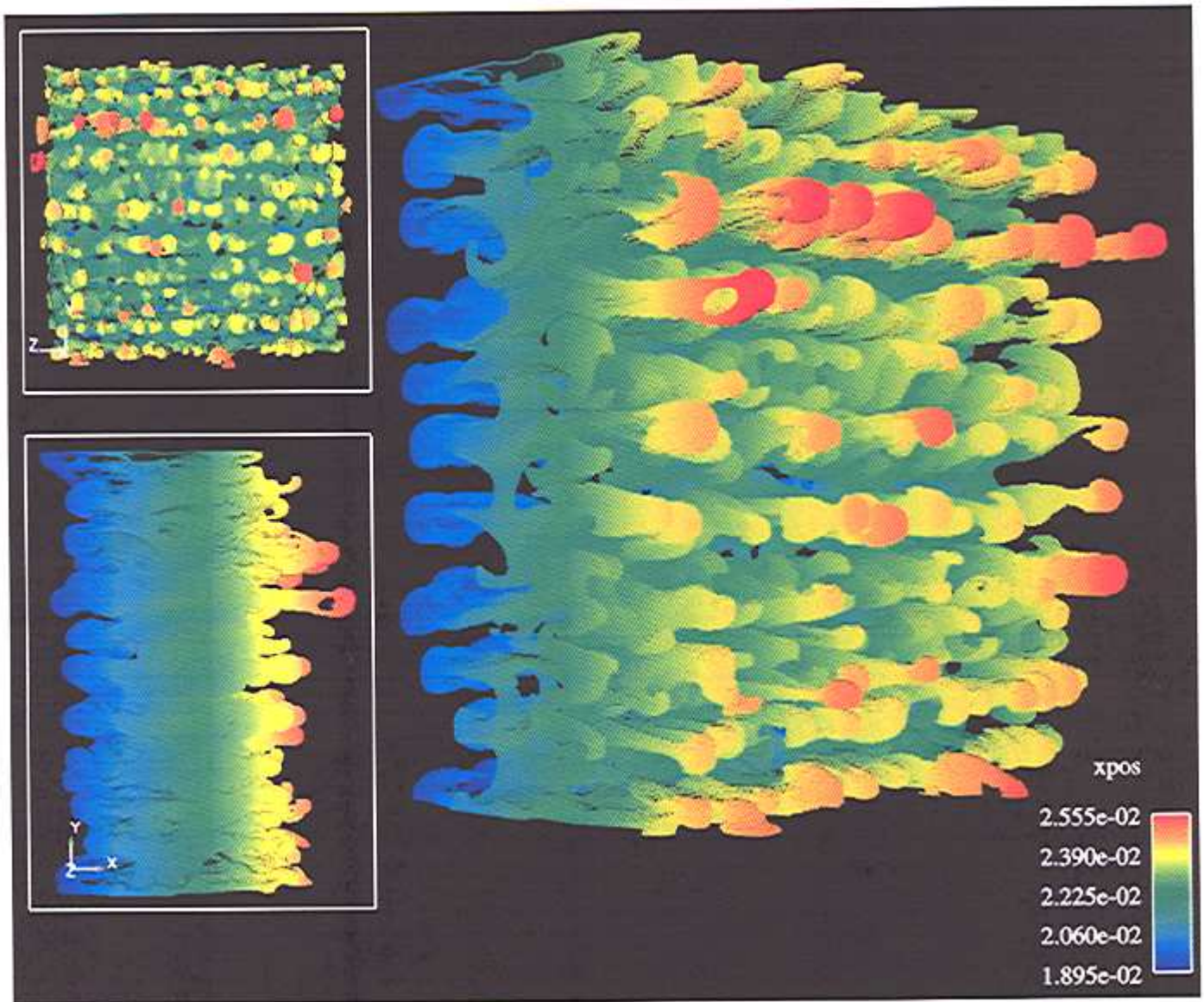


Fig. 9.— Altitude plot showing the specified-rough marker at $t = 4 ns$.

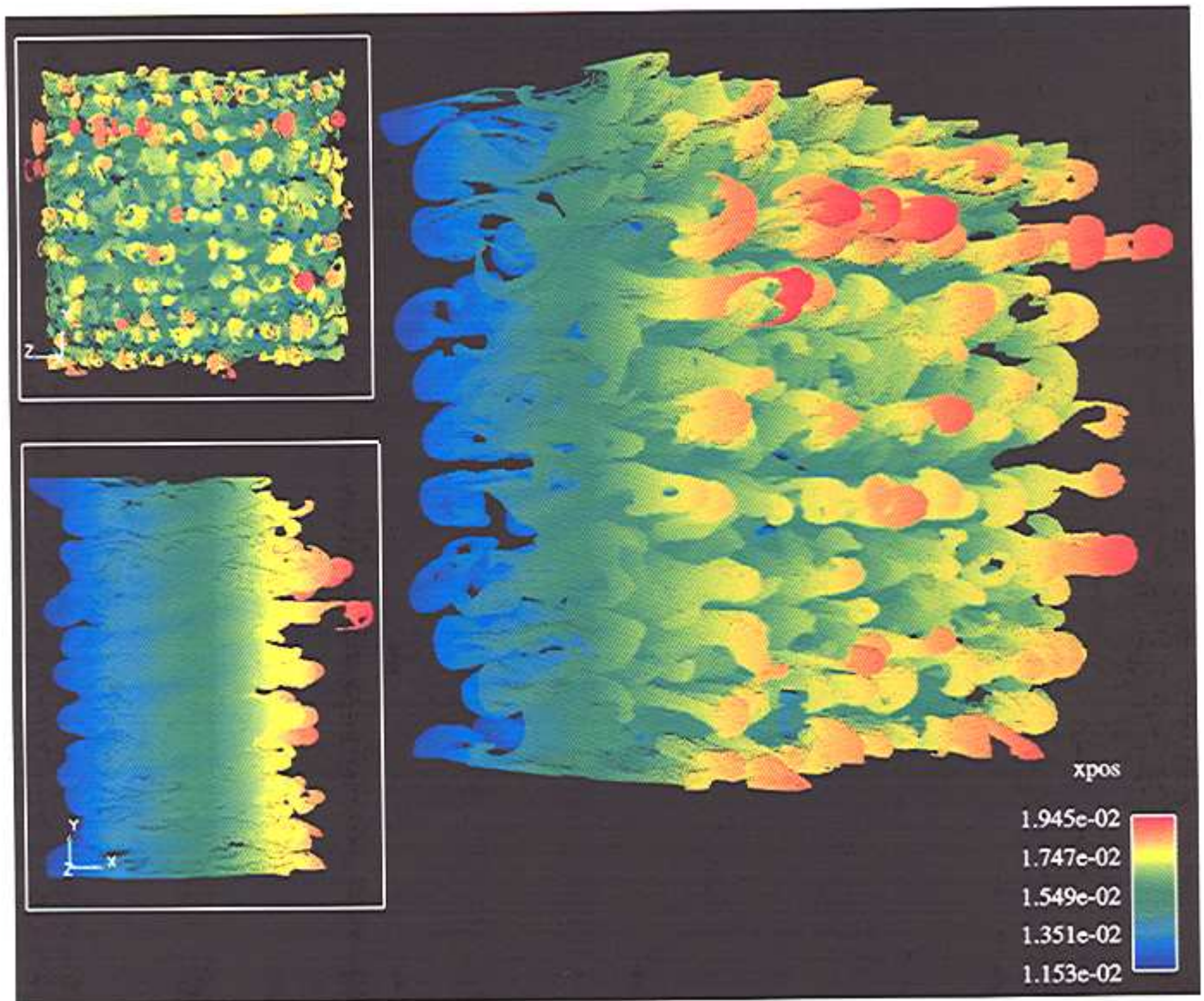


Fig. 10.— Altitude plot showing the specified-rough marker at $t = 5 \text{ ns}$.

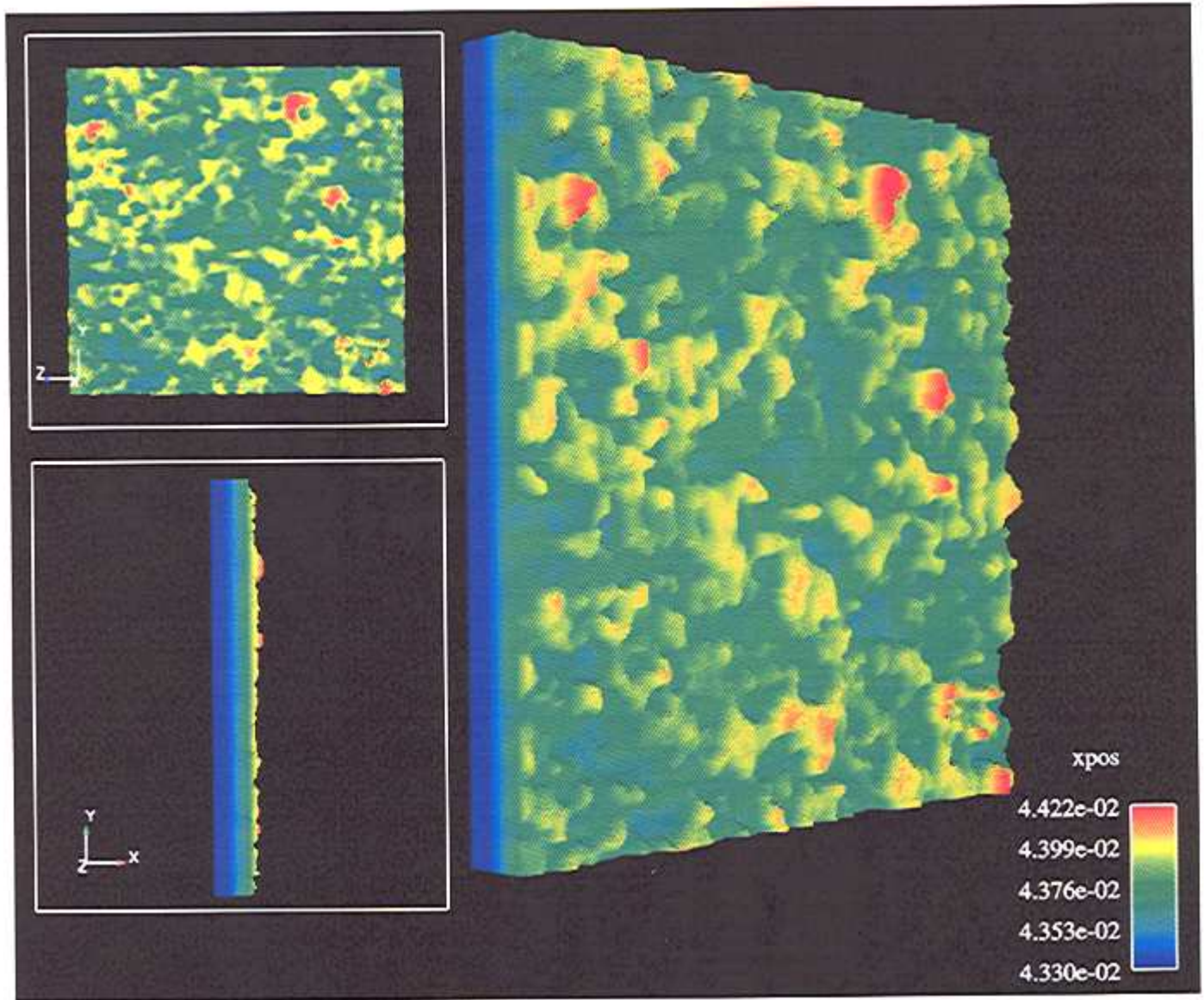


Fig. 11.— Altitude plot showing the super-rough marker at $t = 0$ ns. The color scale shows the x position along the shock tube. The shock passes through the marker in the $-x$ direction.

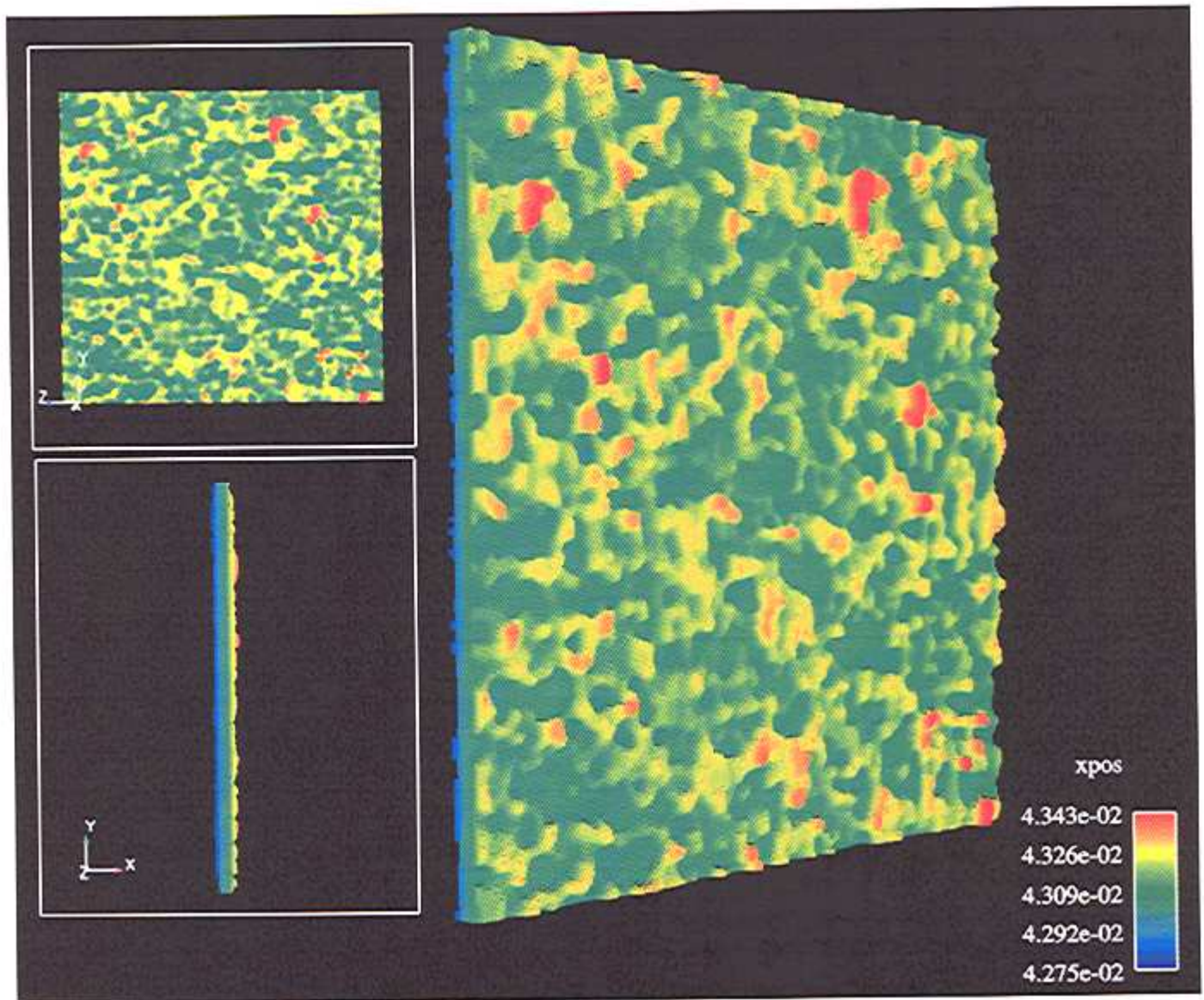


Fig. 12.— Altitude plot showing the super-rough marker at $t = 1 \text{ ns}$.

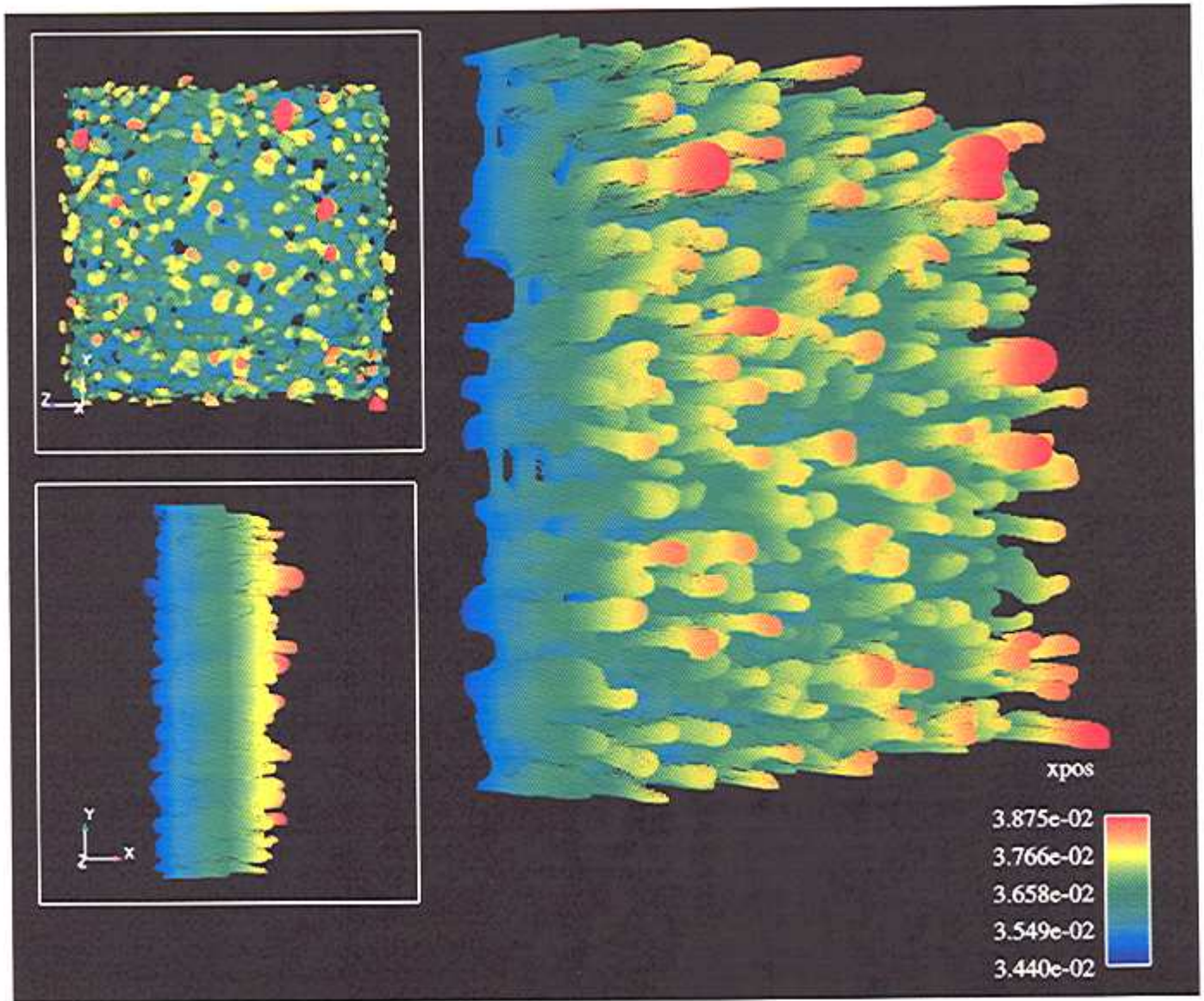


Fig. 13.— Altitude plot showing the super-rough marker at $t = 2 \text{ ns}$.

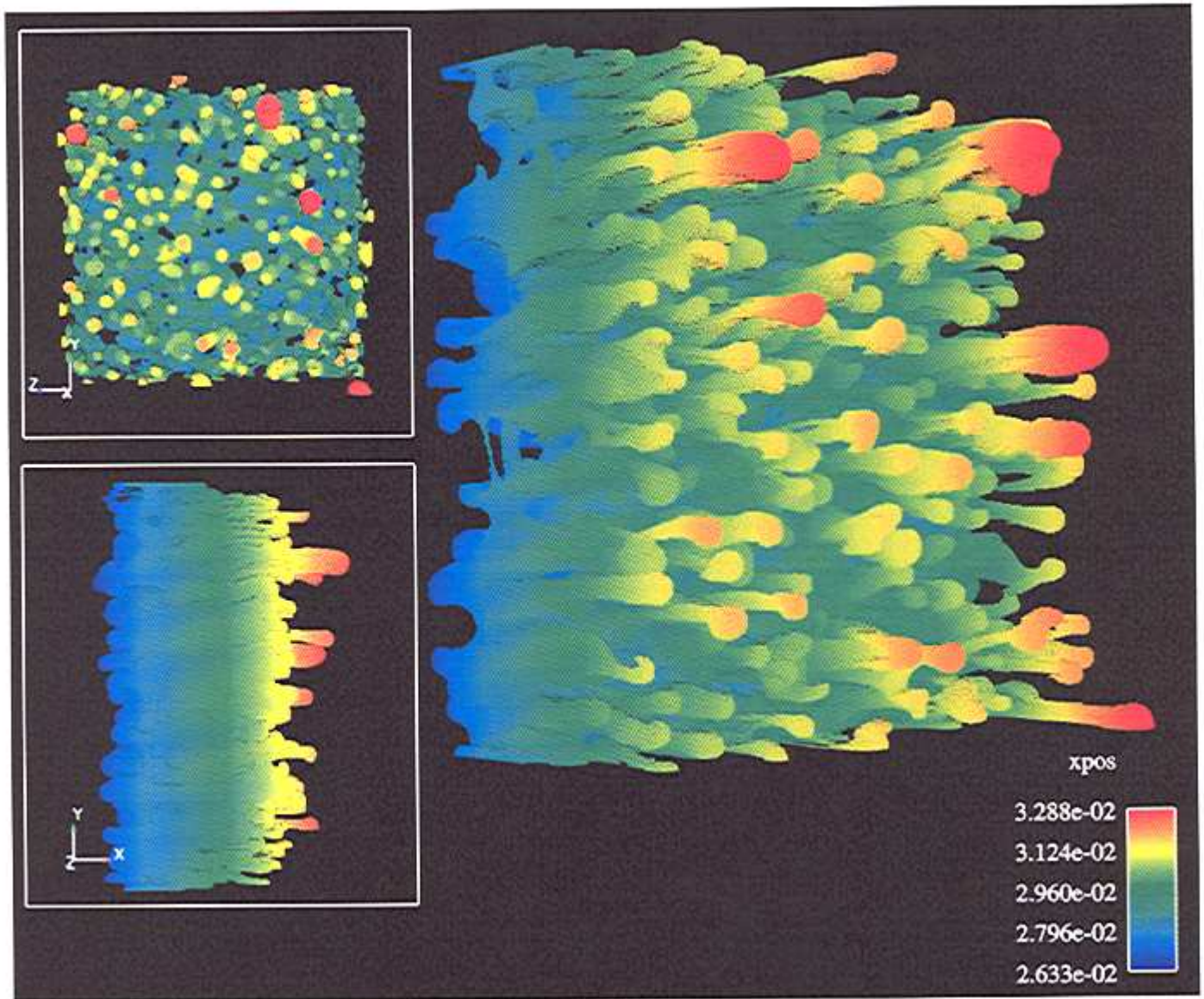


Fig. 14.— Altitude plot showing the super-rough marker at $t = 3 \text{ ns}$.

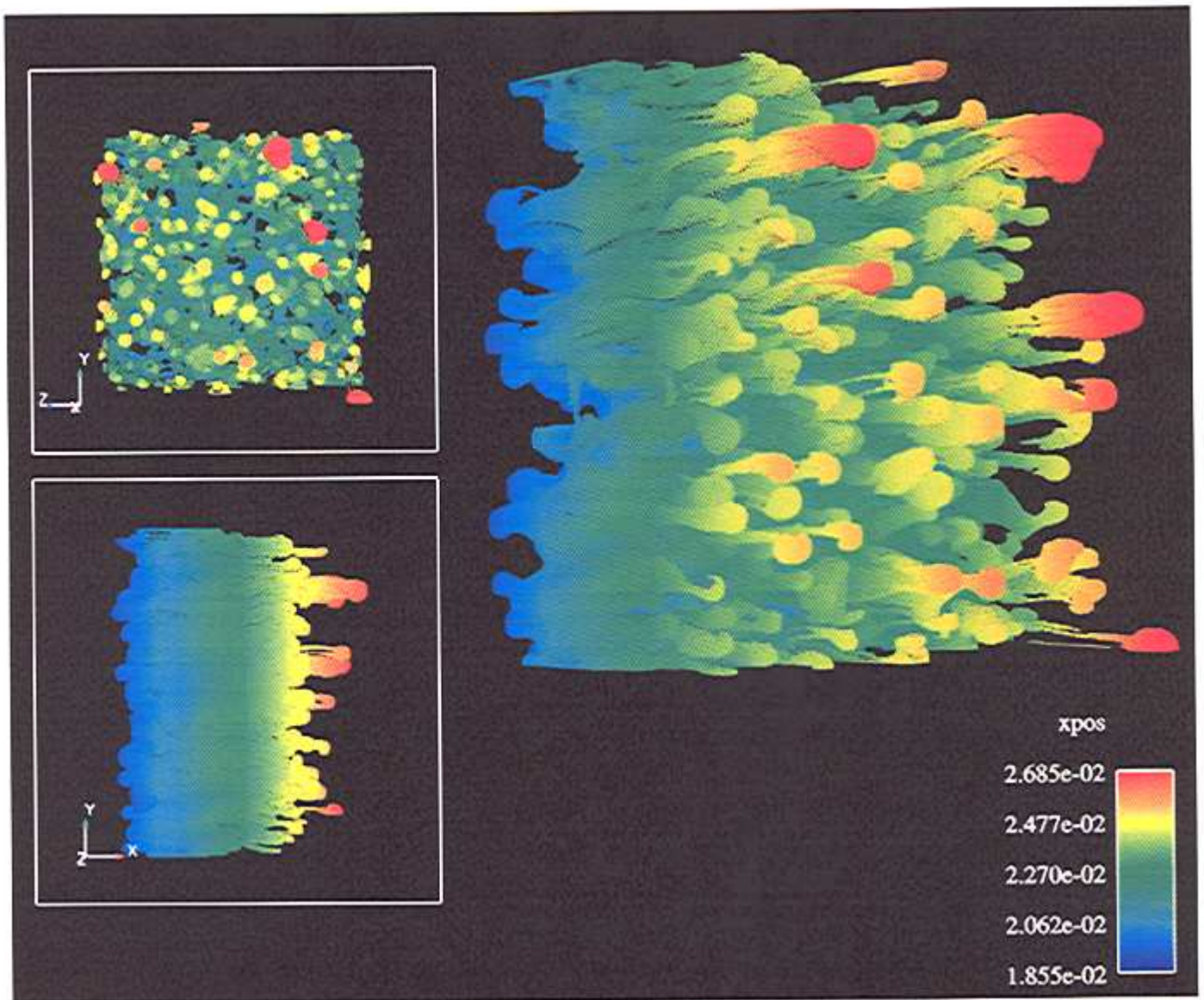


Fig. 15.— Altitude plot showing the super-rough marker at $t = 4 \text{ ns}$.

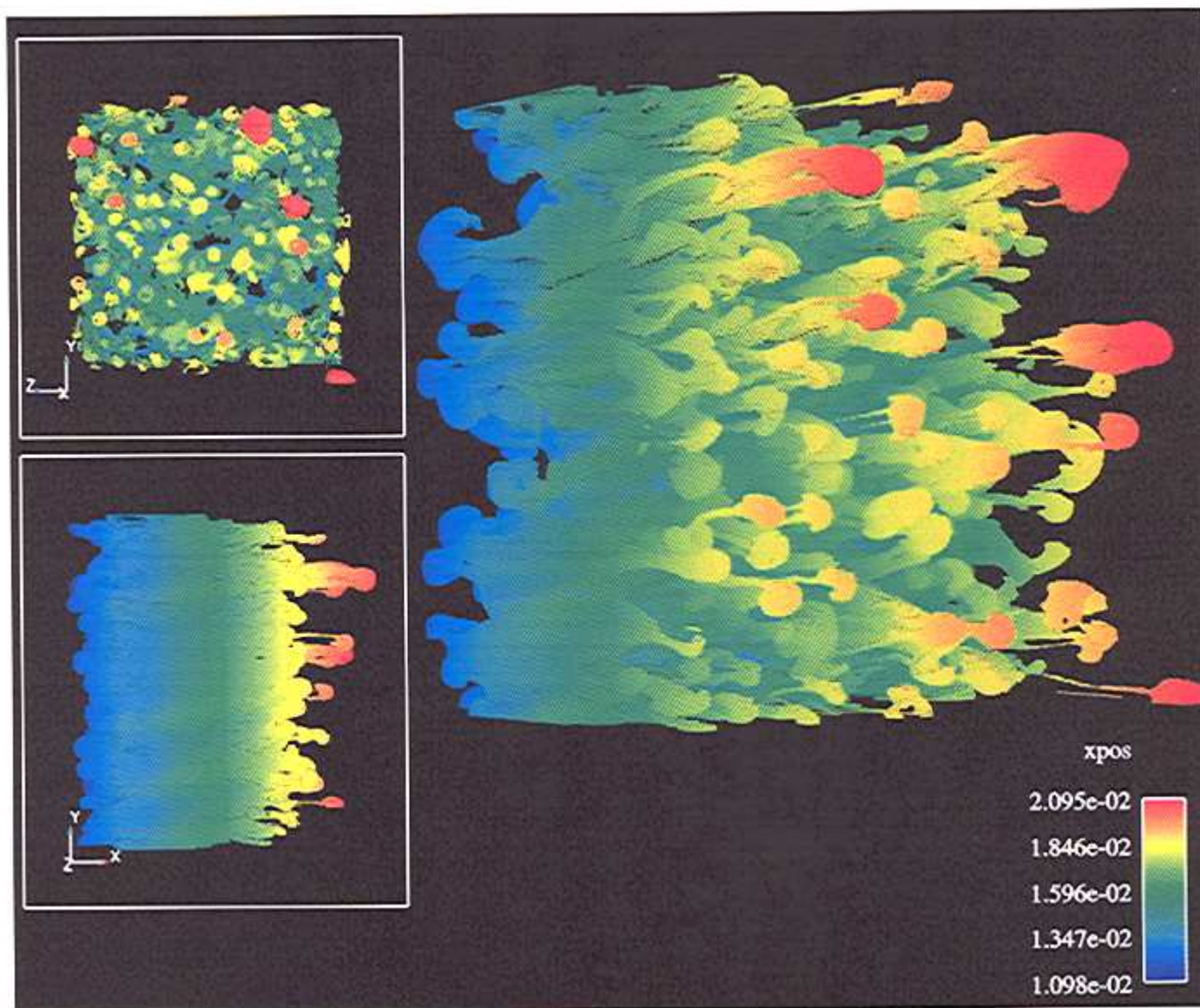


Fig. 16.— Altitude plot showing the super-rough marker at $t = 5 \text{ ns}$.

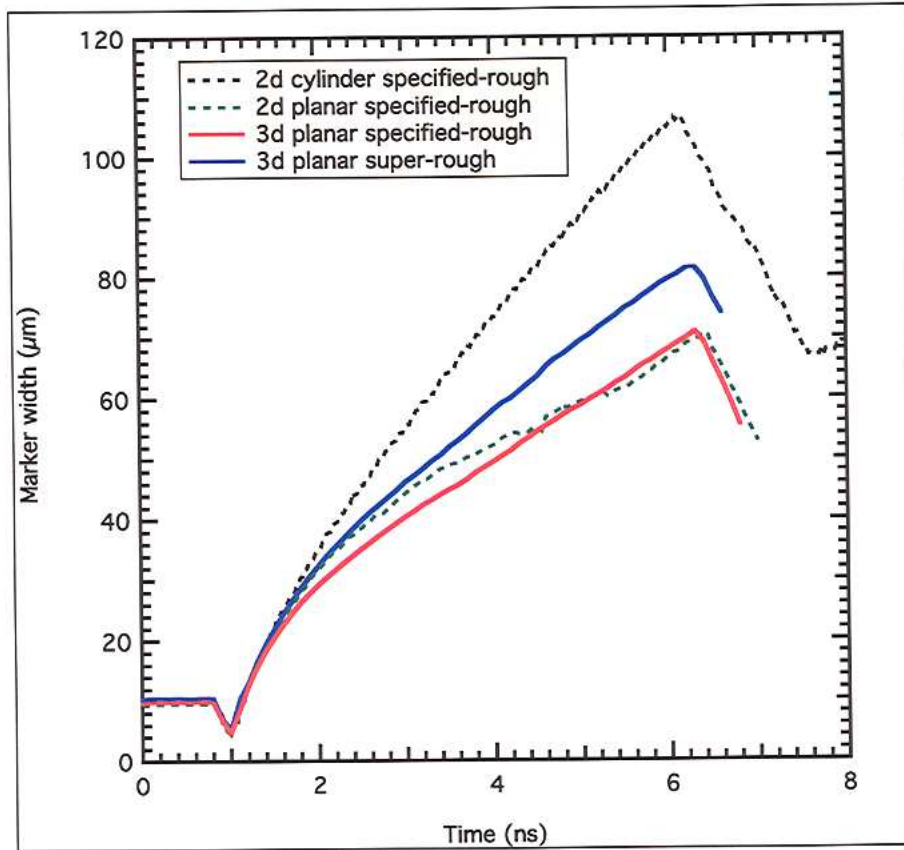


Fig. 17.— Simulated marker-width evolution. The 3-d planar specified-rough (red line) and super-rough (blue line) markers grow in similar fashions. Also shown are a 2-d planar specified-rough case (green dashed line) and the 2-d full cylinder specified-rough case (black dashed line).